Multiphase Chemistry of N_2O_5, $ClNO_2$, and $BrNO_2$

Francis Schweitzer, Philippe Mirabel, and Christian George*

Centre de Géochimie de la Surface/Centre National de la Recherche Scientifique, and Université Louis Pasteur, 28 rue Goethe, F-67083 Strasbourg, France

Received: January 12, 1998; In Final Form: March 10, 1998

The uptake kinetics of N_2O_5 were studied with the droplet train technique as a function of temperature between 262 and 278 K on different aqueous solutions. No pronounced temperature dependence was observed, and the average uptake coefficient in this temperature range is 0.018 ± 0.003. When interacting with salt solutions (i.e., NaCl, NaBr, or NaI), N_2O_5 contributes to the formation of $ClNO_2$ and $BrNO_2$. The multiphase chemistry of these nitryl compounds was further investigated using the wetted-wall technique as a function of temperature between 275 and 293 K on different aqueous solutions. The uptake coefficients are reported for both species, and no distinct temperature dependence was observed. Their uptake rate was efficiently enhanced by the presence, in the aqueous phase, of halogenides ions. When reacting with Br^- or I^-, both nitryl compounds deliver to the gas phase the molecular form of the halogen, i.e., Br_2 or I_2. A reaction scheme potentially explaining these observations is presented and its importance for the sea-salt aerosol chemistry is discussed.

Introduction

Understanding the chemical transformations occurring in the atmosphere is of major societal and intellectual concern because of their potential impact on life. Most of these reactions are driven by free radicals despite their low abundances. Over the past decades, an enormous amount of evidence has been brought to the scientific community for the central role played by odd hydrogen HO_x (i.e., OH and HO_2)[1] in atmospheric oxidation processes of most natural and anthropogenic emitted chemicals including CO, NO_2, and SO_2. However, there is now growing evidence that halogenated radicals may play a significant role in the oxidation capacity of the marine boundary layer (MBL).

It has been shown for a long time that sea-salt aerosols may display a large deficit in chloride compared to the original composition of seawater. Since the mechanisms producing these aerosols (i.e., wave breaking and bubble ejection) should not affect their composition, the observed deficit was generally attributed to the displacement of halogenated inorganic acids due to the uptake, by the aerosols, of strong acids (HNO_3 or H_2SO_4).[2,3] However, in some cases the observed deficit may reach 90% of the original chloride content. As noted by Keene et al.,[4] such a deficit cannot be explained by acid displacement alone. They postulated that other reactions are involved in which stable ions are transformed into halogenated radical precursors. Accordingly, they performed measurements of inorganic chloride in Florida exhibiting HCl* (i.e., HCl plus $ClNO_x$) and Cl_2* (i.e., Cl_2 plus HOCl) concentrations up to 250 ppt with a strong diurnal variation.[5] The latter strongly suggests a night-time buildup of Cl precursors and a subsequent photolysis at dawn. These measured concentrations would correspond to a Cl-atom concentration in the range 10^4-10^5 cm^{-3}, which would imply, for example, a significant enhancement of the oxidation rates of non-methane hydrocarbons (NMHC). Such an enhancement was indeed observed in Lagrangian-type field experiments where it was shown that OH oxidation alone was unable to describe the measured NMHC decay, the latter being consistent with a Cl-atom concentration of about 6×10^4 cm^{-3} at noon.[6]

Although most attention to date has been given to the tropospheric polar O_3 destruction[7,8] (i.e., in a NO_x-free environment), nitrogen oxides chemistry is thought to be essential in a polluted air mass. The reactions that are able to play a role are

$$2NO_2(g) + NaX(s) \rightarrow NOX(g) + NaNO_3(s) \qquad (1)$$

$$N_2O_5(g) + NaX(s) \rightarrow XNO_2(g) + NaNO_3(s) \qquad (2)$$

where the subscripts (s) and (g) denote the solid (or surface-adsorbed) and gaseous states, respectively. In contrast to acid displacement, these reactions lead to the formation of chemically reactive products, which photolyze in the troposphere to atomic halogen.[9−11]

These reactions have already been studied over dry bulk NaCl and NaBr surfaces.[12−16] The available data suggest that the uptake of NO_2 proceeds via $(NO_2)_2$. The tropospheric concentrations of NO_2 are, however, too low to support N_2O_4 formation, and reaction 1 is not believed to be of importance in halogen activation. In contrast, activation by N_2O_5 is certainly a central reaction in this context. In fact, it was assumed that N_2O_5 is hydrolyzed to HNO_3 in the presence of water, leading to a termination reaction for the nitrogen oxide tropospheric cycle. However, Behnke et al.[17] recently showed that this is not the case and that nitryl chloride is produced even in very dilute solutions containing chloride (down to approximately 10^{-2} M). Therefore, the reactions of N_2O_5 with liquid and dry salt aerosols still represent a very effective pathway for the release of photolabile atomic halogen in the marine boundary layer. The formed nitryl halides XNO_2 are then easily photolyzed at dawn or converted to other photolabile species by

$$XNO_2 + NaY \rightarrow XY + NaNO_2 \qquad (3)$$

To get a better insight of halogen activation in polluted regions, it appears crucial to measure the kinetics of reactions 2 and 3 on aqueous solutions. Behnke et al.[17] extensively

* Corresponding author. E-mail: george@illite.u-strasbg.fr.

S1089-5639(98)00748-8 CCC: $15.00
Published on Web 05/06/1998

studied reactions 2 on NaCl-containing solutions and observed a yield close to unity for the production of $ClNO_2$ (reaction 2) and a quite complex chemistry for the nitryl halides, the latter being studied by Frenzel et al.[18]

In the present study, we focused our attention on the uptake rates of N_2O_5, $ClNO_2$, and $BrNO_2$ on different salt solutions chosen to be representative of sea-salt aerosols. The experiments were undertaken using the droplet train and wetted-wall flow tube techniques coupled to different spectrometers enabling a throughout identification of the gas-phase products of reactions 2 and 3.

Experimental Section

The rate of uptake of a trace gas by a liquid is a multistep process that can be related to fundamental properties of the gas, the interface, and the condensed phase such as mass accommodation coefficient (α), solubility, and reactivity. The rate at which a trace gas molecule may be transferred into the condensed phase can be obtained from the kinetic theory of gases. This allows the calculation of the net flux Φ_{net} that may cross the interface

$$\Phi_{net} = {}^1/_4 \langle c \rangle n\gamma \tag{4}$$

where $\langle c \rangle$ is the trace gas average thermal speed, γ is the uptake coefficient (taking into account all processes potentially affecting the uptake rate), and n is the gas-phase density of the trace gas.

The overall principle of measuring γ is very simple; i.e., it consists of exposing an aqueous phase (with a given surface) to the gas under investigation. The major difficulty in these experiments lies in the fact that the surface exposed has to be extremely well-characterized. We developed over the last years the droplet train technique[19] (which was pioneered by the Aerodyne/Boston College Group[20]) in which a surface area of about 0.2 cm^2 is exposed to the gas phase at low pressure. However, for low uptake rates (i.e., $\gamma < 10^{-3}$), this technique is not suitable. Therefore we developed another setup (i.e., a wetted-wall flow tube) in which a surface up to 100 cm^2 may be exposed to the gas phase at atmospheric or low pressure enabling a larger sensitivity for low uptake rates (i.e., $\gamma > 10^{-7}$).

The Droplet Train Technique. The technique used to measure the uptake rates has already been described elsewhere,[19] and therefore we will only provide a brief summary of its principle of operation. The uptake coefficient is measured by the decrease of the gas-phase concentration of the trace species, owing to their exposure to a monodisperse train of droplets. These latter are generated by a vibrating orifice (75 μm diameter) leading to droplet diameters in the range 80−150 μm.

The apparatus, where the contact between both phases takes place, is a vertically aligned flow tube whose internal diameter is 1.8 cm. Its length can be varied up to 20 cm, in order to change the gas/liquid interaction time (0−20 ms) or the surface exposed by the droplet train (0−0.2 cm^2). Since the uptake process is directly related to the total surface S exposed by the droplets, any change ΔS in this surface results in a change Δn of the trace gas density at the exit ports of the flow tube. In fact, by considering the kinetic gas theory, it becomes possible to calculate the instantaneous uptake rate as

$$\frac{dn}{dt} = -\frac{\langle c \rangle}{4}\gamma_{obs} n \frac{S}{V} \tag{5}$$

where γ_{obs} is the experimental uptake coefficient and V the volume of the interaction chamber. However, since we are measuring the averaged signal during the transit time due to changes in the exposed surface, eq 5 has to be integrated leading to[20]

$$\gamma_{obs} = \frac{4F_g}{\langle c \rangle \Delta S} \ln\left(\frac{n}{n - \Delta n}\right) \tag{6}$$

where F_g is the carrier gas volume flow rate and n and Δn are, respectively, the trace gas density at the inlet and outlet port of the interaction chamber. Typical experimental values for F_g are in the range 200−650 mL min^{-1} STP. By measuring the fractional changes in concentration $[n/(n - \Delta n)]$ as a function of $\langle c \rangle \Delta S/4F_g$, it becomes possible to determine the overall uptake coefficient γ_{obs}. This parameter can be measured as a function of the total pressure, gas/liquid contact time, or composition of the liquid used to produce the droplets. These last measurements are necessary to decouple the overall process into individual steps.

An important aspect of this technique is the careful control of the partial pressure of water in the flow tube since it controls the surface temperature of the droplets through evaporative cooling.[20] Therefore, the carrier gas (helium) is always saturated, at a given temperature, with water vapor before entering the flow tube. The equilibrium between ambient saturated helium and the liquid droplets is reached in the first zone of the setup before the interaction zone. The liquid used to produce the droplets was thermostated up to the orifice, for temperatures larger than 0 °C, leading to fast equilibrium attainment. Temperatures lower than 0 °C were obtained through evaporative cooling of the droplets in the first part of the flow tube. At these lower temperatures, the droplets are supercooled but not frozen even for temperatures lower than −20 °C.[20] However, for supercooled droplets the temperature refers to the surface thermal equilibration, which occurs within a time scale of about 1 ms and is therefore obtained before the droplets reach the region where they are exposed to the trace gases. Thermal conduction for our droplets has a characteristic time of about 10 ms, meaning that although the surface quickly equilibrates with the ambient water vapor, the interior of the droplets' volume will not be at equilibrium. As shown by Worsnop et al.,[20] the measured uptake rate is therefore an average over a range up to 3 K around the desired temperature (including an uncertainty of 10% on the water partial pressure).

The Wetted-Wall Flow Tube. This technique has been used to study the transport of gases into liquids for many years.[21] The approach employed to obtain the uptake kinetics is very similar to the one of the droplet train technique, but it takes advantage of the fact that the well-described mass transport equation in cylindrical coordinates can be applied.

The uptake kinetics were measured by the loss rate of the gas species flowing along a vertically aligned flow tube, the walls of which are covered by a film of a slowly flowing down aqueous solution. A schematic diagram of our apparatus is given in Figure 1. The flow tube itself is made of a 1 m long glass tube with an internal diameter d_{tube} of 1.2 cm. The temperature of the glass was maintained constant by flowing around it a water−ethanol mixture from a temperature-controlled bath. The aqueous solutions used to produce the film were also thermostated at the same temperature. The movable gas in- and outlet were made of approximately 1.2 and 0.8 cm (o.d.) Teflon tubbings. The gas flowed through these tubbings whereas the liquid passed between the inner glass walls of the flow tube and the outer walls of the inlet Teflon tubbings. This gas inlet was designed in such a way that the water could be forced, from a small reservoir at the upper end of the flow tube, through the available space between the glass and Teflon walls.

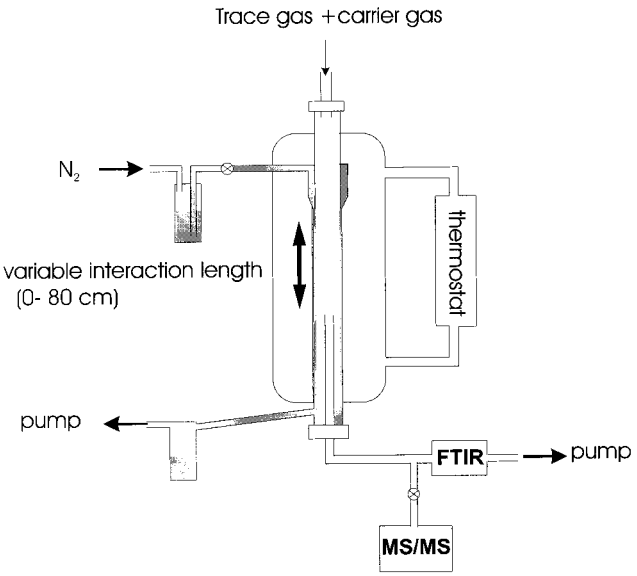

Figure 1. Schematic representation of the wetted-wall flow tube.

This free space was so restricted that this operation led to a liquid film that completely wetted the glass walls. The obtained film then slowly flowed down under the effect of gravity. To ensure that the glass was always wetted over the length of the flow tube, the latter was daily rinsed with concentrated NaOH solutions and then with Milli-Q (18 MΩ) water. In addition, the flow tube was filled with a concentrated NaOH solution overnight. This procedure was found to give clean glass surfaces that were easily wetted with aqueous solutions. The liquid flowed out of the flow tube between the glass tube and the movable gas outlet and was stored in an evacuated glass vessel.

The helium carrier gas flow (in the range from 140 to 200 mL min^{-1} STP) was controlled by calibrated electronic mass flow meters. This gas was always saturated with water vapor at the temperature of the liquid film by passing through thermostated water bubblers before entering the flow tube. This step was necessary in order to avoid any potential evaporation of water vapor from the liquid film that would cool the latter below the temperature of the water−ethanol mixture. However, this was always avoided, and the temperature of the film was also assumed to be the same as the cooling bath.

This wetted wall flow tube was operated at atmospheric pressure but also at reduced pressure, and in such a case the flow tube was connected to a pumping system. The pressure range used in theses experiments was varied from 15 to 30 Torr and was measured with capacitance manometers that could be connected to different positions (i.e., at the inlet, outlet, water bubblers) in order to control the pressure gradient in the tubings or flow tube.

The dynamics of a liquid film flowing down under the effect of gravity has already been presented by Danckwerts.[21] The thickness of the film f can be calculated according to

$$f = \left(\frac{3\eta F_1}{\pi g d_{\text{tube}} \rho}\right)^{1/3} \tag{7}$$

where η and ρ are the viscosity and density of the aqueous solution and F_l is the liquid flow rate. The latter was measured by a calibrated rotameter and it was in the range 2−6 mL min^{-1}, giving a film thickness in the range from 6.1×10^{-3} to 1.2×10^{-2} cm.

To ensure that the mass transport in the gas can be described by diffusion processes alone, i.e., without being disturbed by turbulences produced by ripples on the film surface's, one has to ensure that the liquid flow is laminar. This was done by keeping the liquid flow rate as low as possible. In fact, for all experiments reported here, we never observed the presence of ripples on the film surfaces (however, with higher flow rates they were indeed present and visible). Another indicator for the presence of turbulence in the liquid film is given by the Reynold's number N_{Re} defined by

$$N_{\text{Re}} = \frac{F_1 \rho}{\pi d_{\text{tube}} \eta} \tag{8}$$

Using this equation, we calculated a Reynold's number smaller than 3, a value far below the limit of 250−400 where turbulent transport is present. Therefore and with the nonobservation of ripples, we assumed that gas-phase transport can be described by diffusion alone.

The trace gas loss rate in the flow tube was measured as a function of the position of the movable outlet, i.e., as a function of the gas/liquid exposure time t. The length l of the interaction zone could be varied up to 80 cm. As will be shown below, the measured loss rate was always first order with respect to the gas-phase concentration of the reacting species, i.e.

$$\frac{n - \Delta n}{n} = \exp[-k_{\text{w}} t] \tag{9}$$

where t is the average gas residence time and k_{w} is the first-order rate constant for the reactions at the liquid film surface. By taking into account the geometric liquid surface exposed to the gas phase and the volume of the flow tube, one can extract, from eq 9 after time integration, an expression for k_{w}

$$k_{\text{w}} = \frac{\gamma \langle c \rangle}{2 r_{\text{tube}}} \tag{10}$$

where r_{tube} is the flow tube radius. However, this equation is not valid if gas-phase diffusion limitations are present, i.e., when radial gas concentration profiles build up. To take into account gas-phase diffusion, we used the Cooney−Kim−Davis (CKD) equation[22,23] as described by Behnke et al.[17]

$$(n - \Delta n)/n = B_1 \exp(-\Lambda_1^{\,2} z^*) + B_2 \exp(-\Lambda_2^{\,2} z^*) + \ldots \tag{11}$$

where B_i and Λ_i are functions of the Sherwood number N_{shw}, which is defined as

$$N_{\text{shw}} = \frac{r_{\text{tube}} \langle c \rangle}{4 D_{\text{g}}} \left(\frac{\gamma}{1 - \gamma/2}\right) \tag{12}$$

and where z^* is a dimensionless reaction length

$$z^* = l \frac{D_{\text{g},0}}{2 F_{\text{g}}^0} \frac{T}{T_0} \tag{13}$$

In eqs 11−13, γ represents the corrected uptake coefficient, l is the reaction length, D_{g} is the binary gas diffusion coefficient, T is the temperature, and F_{g} is the gas flow rate ($cm^3\ s^{-1}$). The subscript 0 refers to the standard conditions. Values of B_i and Λ_i were taken from the table given by Murphy and Fahey[23] interpolated from the four nearest values of N_{shw} by a cubic polynomial as suggested by Behnke et al.[17]

By using eq 11, which was shown to give the same results as the methodology developed by Brown,[24] we could check if our experiments were affected by gas-phase diffusion limitations. It appears that for all the experiments reported here, these limitations were very small and the uptake coefficients calculated with the simple eq 10 were very closed to the results of the more detailed eq 11.

Analytical Methods and Gas Production. An ion-trap mass spectrometer (Varian model Saturn 4D) and a FTIR spectrometer (Nicolet Protégé 460 equipped with an IRA long path White-cell; light path ranging from 2.2 to 22 m) were connected to the exit ports of the different flow tubes. These spectrometers were systematically used together in the course of this work in order to ensure a complete analysis of the gas flow.

Aqueous solutions used to prepare the droplets were made from Milli-Q water (18 MΩ cm) and reagent-grade salts when necessary. N_2O_5 was produced as a continuous gas stream by reacting NO with an excess ozone. For this purpose, a flow of helium containing 10 000 ppm NO (Alphagaz) was mixed in a tubular vessel with O_3 produced by an electric discharge generator (Sorbios model GSG 001.2) from a flow of pure O_2 (Prodair, 99.95%). Both gas streams were dried over P_2O_5 or $CaSO_4$. To stabilize N_2O_5 in the gas phase and to complete the reaction, O_3 was used in excess. Nitryl chloride was prepared by adding chlorosulfonic acid (Fluka, >98%) dropwise to practically anhydrous nitric acid (Fluka, 100%) at room temperature.[25] The gas that evolved was collected in a trap cooled at the temperature of liquid nitrogen leading to a white solid, which was further purified by pumping off the vapor in an evacuated trap during warming. This material was then stored around 200 K with negligible loss over weeks. At that temperature, the solid melts into a very pale greenish-yellow liquid, and in order to produce a continuous source of $ClNO_2$, a small flow of helium was allowed to pass above the liquid and entrained the $ClNO_2$ vapor. The gas was then analyzed by mass and IR spectrometry, and it was found that it was nearly pure $ClNO_2$ with little Cl_2 impurities. Nitryl bromide was continuously synthesized by heterogeneous reaction of Br_2 with a 0.005 mol/L aqueous $NaNO_2$ solution in a wetted-wall flow tube as described by Frenzel et al.[18] For this operation, a flow of helium containing molecular bromine (Acros Organics, >99,8%) at mixing ratios in the range from 460 to 740 ppm was fed into a thermostated flow tube whose inner walls were covered by a $NaNO_2$ solution. The reaction length, about 15 cm, was long enough to convert almost all Br_2 into $BrNO_2$ and short enough to avoid the destruction of $BrNO_2$ by reaction with $NaNO_2$. This flow of helium containing $BrNO_2$ and Br_2 was then allowed to enter the flow tube where the uptake kinetics of $BrNO_2$ was investigated. The thermal lifetime of $BrNO_2$ was measured in a glass cell with silice windows at room temperature (i.e., 298.35 K) to be 49 min in close agreement with the data reported by Frenzel et al.[18] Note, however, that this lifetime may be efficiently shortened by the presence of reactive surfaces (such as metallic fittings, etc.), which destroy the nitryl bromide heterogeneously. This observation is in agreement with those of Frenzel et al.,[18] who identified from the temperature dependence of the lifetime that it is probably affected by heterogeneous wall losses.

Figure 2 gives the infrared spectra measured for N_2O_5, $ClNO_2$ and $BrNO_2$ between 650 and 2000 cm^{-1} (in each case, 32 spectra were co-added in order to increase the S/N ratio). All these spectra are in close agreement with those of the literature.[26−28]

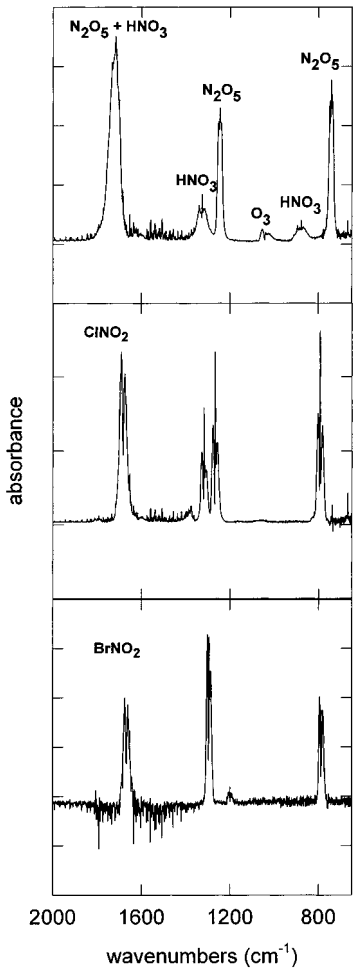

Figure 2. Typical infrared spectra of N_2O_5, $ClNO_2$, and $BrNO_2$. (32 scans were coadded.) When impurities are present, the corresponding bands are marked; otherwise, the bands correspond to the stated compound.

Results

Dinitrogen Pentoxide. The uptake of N_2O_5 by different aqueous solutions was reinvestigated, as a function of temperature by the droplet train technique between 262 and 278 K. The uptake coefficients were determined using eq 6 (a typical plot of a first-order uptake kinetic is given in Figure 3) and corrected for gas-phase diffusion limitations according to

$$\gamma = \frac{1}{\frac{1}{\gamma_{obs}} - \frac{\langle c \rangle d_{eff}}{8D_g} - \frac{1}{2}} \tag{14}$$

where d_{eff} is the effective droplet diameter.[20] The diffusion coefficient (D_g) is not known and therefore had to be estimated by the method presented by Reid et al.[29] In addition, since our carrier gas is a mixture of helium and water vapor, it was necessary to compute the diffusion coefficient in this background. This was done according to the following equation

$$\frac{1}{D_g} = \frac{P_{H_2O}}{D_{g-H_2O}} + \frac{P_{He}}{D_{g-He}} \tag{15}$$

where P_{H_2O} and P_{He} are the partial pressures of water and helium respectively, D_{g-H_2O} and D_{g-He} are the binary diffusion coefficients of the trace gases in water and helium, respectively. The uptake coefficients corrected for diffusion limitations are

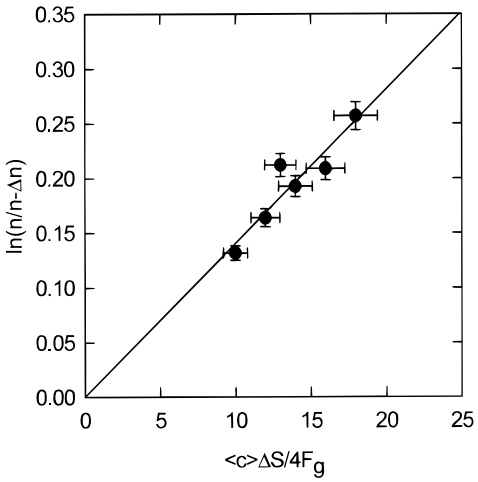

Figure 3. Typical plots of $\ln(n/n - \Delta n)$ versus $\langle c \rangle \Delta S/4F_g$ for N_2O_5 on pure water at 275 K. According to eq 6, the slopes of such plots are a measure of the uptake coefficient γ. The solid line represents a linear fit to our data. The errors of the individual measurement are estimated to be less than 15% (including 4, 5, and 5% uncertainties on the droplets' surface, determination of the relative decay, and gas flow rates, respectively).

TABLE 1: Uptake Coefficients γ of N_2O_5 on Water and Different Salt-Containing Solutions

solution	temp	$\gamma \pm 2\sigma$
water	264	0.021 ± 0.005
	268	0.021 ± 0.003
	273	0.018 ± 0.007
	275	0.015 ± 0.006
1 M NaCl	262	0.017 ± 0.015
	266	0.014 ± 0.008
	270	0.017 ± 0.005
	273	0.012 ± 0.002
	278	0.014 ± 0.007
1 M NaCl + 10^{-1} M NaBr	270	0.018 ± 0.006
	271	0.017 ± 0.003
	276	0.011 ± 0.002
	277	0.015 ± 0.004
10^{-1} M NaBr	271	0.023 ± 0.006
1 M NaBr	272	0.021 ± 0.013
10^{-2} M NaBr	272	0.018 ± 0.004
	276	0.021 ± 0.004
1 M NaI	271	0.017 ± 0.001
10^{-1} M NaI	272	0.024 ± 0.004
	277	0.023 ± 0.003
1 M NaCl + 10^{-2} M NaBr + 10^{-4} M NaI	272	0.022 ± 0.003
10^{-1} M NaI	276	0.022 ± 0.004

listed in Table 1 for all solutions studied here. The results on pure water and a 1 M NaCl solution are also given in Figure 4. The values measured for pure water and on 1 M NaCl solution are very close to those reported in the literature (including our previous study).[30−33] It is, however, difficult to assess any temperature dependence that, if it exists, must be lower than previously reported.

Another salient feature of our results can be obtained by comparing the results for the different solutions. In fact, despite the large differences in reactivity between Cl^-, Br^-, and I^-, no significant change in the uptake coefficient was measured. For all solutions at all temperatures studied, the uptake coefficients were comparable. Therefore we can report an average value of $\gamma = 0.018 \pm 0.003$ between 262 and 278 K (the same average value is obtained when including our previous work[33]). To explain the independence of γ with the composition of the aqueous phase, we can discuss several possibilities. First, we could have measured the maximum rate of mass transfer for N_2O_5; i.e., the uptake coefficients listed in Table 1 are then equal

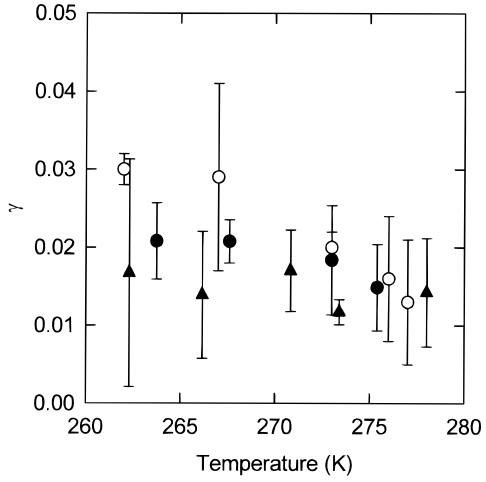

Figure 4. Plot of γ versus temperature for N_2O_5. The error bars are given at the 2σ level. Circles, pure water; triangles, 1 M NaCl; hollow circles, data on pure water from ref 33.

to the mass accommodation α. In such a situation, the uptake rate would had been insensitive to the presence of a scavenger and in addition, α would be temperature-dependent (exhibiting a negative temperature dependence[34]), which was not observed. Second and more realistically, the reactants we added to the liquid phase were either nonreacting at all or nonreacting directly with aqueous molecular N_2O_5 but with its dissociation and/or hydrolysis products. In older and recent studies,[35,36] it has been shown that the uptake rate of N_2O_5 on acidic solutions does not depend on its water content; therefore, it was postulated that dinitrogen pentoxide first dissociates, in a rate-limiting step, according to

$$N_2O_{5(aq)} \leftrightarrow NO_2^+ + NO_3^- \qquad (16)$$

Such a reaction was previously observed as a decomposition pathway for N_2O_5 in concentrated protic inorganic solvents as demonstrated by Raman spectroscopy.[25] Recently, Behnke et al.[17] showed that this reaction also occurs in dilute aqueous solutions and that it is followed by reaction of the highly reactive nitronium ion with X^- (where X is Cl and Br) or water according to

$$NO_2^+ + H_2O \rightarrow 2H^+ + NO_3^- \qquad (17)$$

$$NO_2^+ + X^- \rightarrow XNO_2 \qquad (18)$$

The succession of these reactions is in agreement with our observations that the uptake rate is independent of the concentration of X^- since these ions are not reacting with aqueous molecular N_2O_5.

Another indirect confirmation that reactions 16−18 effectively occurred in our system is obtained by the identification of the gas-phase products using both mass and FTIR spectrometers. With a 1 M NaCl solution, we effectively observed nitryl chloride as the unique gas-phase product in agreement with the studies of Behnke et al.[17] We also determined from the loss and appearance of N_2O_5 and $ClNO_2$ that the yield of the latter is very close to unity, i.e., 1.00 ± 0.14 (at the 2σ level). In NaBr solutions, we observed $BrNO_2$, Br_2, and HONO as products of the interaction of Br^- with N_2O_5. Finally, for NaI solutions the unique gas-phase product was I_2. The observation of different products beside the nitryl halides is evidence that these latter react also with the aqueous droplets.

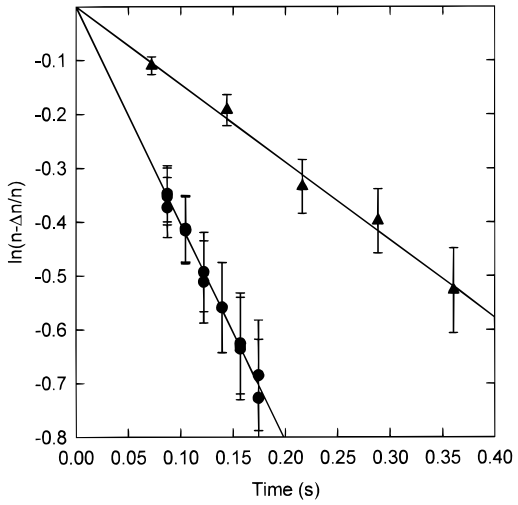

Figure 5. Typical relative decay of $ClNO_2$ and $BrNO_2$ as measured in the flow tube. For $ClNO_2$ the kinetics were measured on 10^{-2} M NaBr solution at 281 K (triangles), whereas the data for $BrNO_2$ were measured on a 10^{-4} M NaI solution at 282 K. The slope of the straight line is related to the uptake coefficient γ. The errors of the individual measurement are estimated to be less than 15% (including 5% uncertainties for determination of the relative decay and gas flow rates respectively).

Nitryl Chloride. The uptake of nitryl chloride was beyond the detection limit of the droplet train technique, i.e., its uptake coefficient for all the solutions we investigated (up to 1 M NaBr) was below 10^{-3}, and in order to overcome this problem, we used for the nitryl halides the wetted-wall flow tube technique, which has a larger sensitivity for low uptake rates. We studied the uptake of $ClNO_2$ on NaBr and NaI solutions as a function of temperature between 275 and 289 K. A typical first-order plot obtained by this technique is given in Figure 5, and the complete set of results is listed in Table 2. By considering these data, it is clear that the uptake of $ClNO_2$ is strongly influenced by the composition of the aqueous phase. In such a case, the uptake coefficient can adequately be described by

$$\frac{1}{\gamma} = \frac{1}{\alpha} + \frac{\langle c \rangle}{4HRT\sqrt{kD_a}} \qquad (19)$$

where α is the mass accommodation coefficient, H is the Henry's law constant, R is the gas constant, D_a is the aqueous-phase diffusion coefficient, and k is the first-order rate constant for the chemical reaction occurring in the liquid phase. Therefore a plot of $1/\gamma$ versus $[NaX]^{-1/2}$, should lead to a straight line. This is indeed the case as depicted by Figure 6 at 275 K for NaBr solutions. It can also be seen from this figure that the intercept is negligibly small, i.e., $\alpha \gg \gamma$. Therefore eq 19 can be simplified to

$$\gamma \approx \frac{4HRT\sqrt{kD_a}}{\langle c \rangle} \qquad (20)$$

Using estimated aqueous-phase diffusion coefficients,[29] it is possible to calculated values for the product $Hk^{1/2}$ that are listed in Table 3. The data reported here are in close agreement with data measured nearly simultaneously by two other groups with the same technique[18,37] and with our previous study with the droplet train technique[38] where we observed that iodide is an efficient scavenger for $ClNO_2$ and that the reaction leads to the formation of NO_2^- and I_2. In this work, we reported a very small temperature dependence, which is not observed in the present study with the wetted-wall flow tube. It seems to us that the experimental control of the setup was greatly enhanced since our former work; therefore, the data reported here should be considered as the most accurate. A temperature-independent reactive uptake rate may be explained by the opposite dependence of the rate constant and solubility with temperature.

It should be underlined that, whereas the intercept of a plot of $1/\gamma$ versus $[NaX]^{-1/2}$ was always zero for NaBr solutions, it was always slightly negative for NaI solutions as we already reported from studies with more concentrated solutions.[38] It was postulated that this negative intercept may be evidence of surface reaction between I^- and $ClNO_2$. The same feature appeared again in the present study while using totally different

TABLE 2: Uptake Coefficients γ of $ClNO_2$ on Different Salt-Containing Solutions

solution	temp	$(\gamma \pm 2\sigma) \times 10^6$
10^{-4} M NaBr	275	7.1 ± 1.9
	279	5.3 ± 0.4
	282	5.9 ± 1.2
	288	8.6 ± 1.7
10^{-3} M NaBr	275	26.0 ± 7.9
	279	20.2 ± 4.0
	282	14.3 ± 4.5
	288	18.0 ± 5.0
10^{-2} M NaBr	275	80.7 ± 7.8
	279	94.0 ± 11.4
	282	63.4 ± 7.5
	288	90.1 ± 12.0
10^{-1} M NaBr	275	400 ± 7
	279	294 ± 4
	282	270 ± 4
	288	310 ± 7
1 M NaBr	275	919 ± 78
	279	834 ± 16
	282	832 ± 15
	288	935 ± 148
10^{-4} M NaI	275	30.8 ± 11.0
	279	32.1 ± 6.9
	284	34.6 ± 26.3
	288	34.6 ± 0.9
10^{-3} M NaI	275	933 ± 170
	279	1022 ± 229
	282	1205 ± 325
	288	980 ± 36
10^{-2} M NaI	275	4530 ± 279
	279	3790 ± 421
	284	2720 ± 573
	288	3910 ± 74

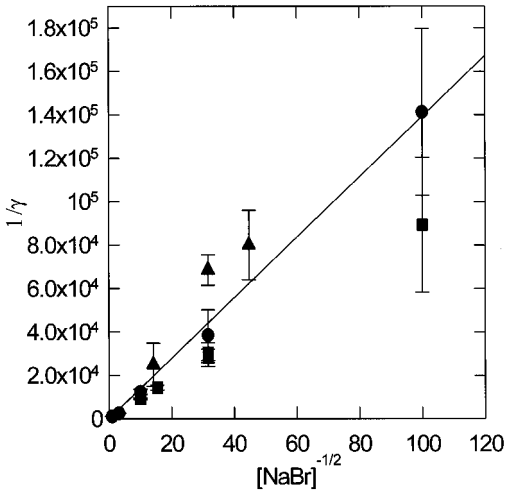

Figure 6. Plot of γ^{-1} versus $[NaBr]^{-1/2}$ for $ClNO_2$ on NaBr solutions according to eq 19 at 275 K. Circles, this work; triangles, Frenzel et al. (ref 18); squares, Crowley et al. (ref 37).

TABLE 3: Values of the Product $Hk^{1/2}$ for $ClNO_2$ and $BrNO_2$ on Different Salt-Containing Solutions As Derived from the Uptake Coefficient Measurements[a]

	temp	$Hk^{1/2}$
$ClNO_2$ + NaBr	275	103.1 ± 18.7
	279	83.5 ± 4.12
	282	80.3 ± 2.5
	288	81.3 ± 1.8
$ClNO_2$ + NaI	275	4384.7 ± 326.7
	282	3933.1 ± 170
	288	4379.6 ± 34.4
$BrNO_2$ + NaCl	278	0.51 ± 0.13
	282	0.78 ± 0.26
	285	1.03 ± 0.22
	288	1.06 ± 0.25
	293	0.81 ± 0.22
$BrNO_2$ + NaBr	278	47.7 ± 15.2
	282	51.9 ± 18.0
	285	53.1 ± 7.8
	293	62.9 ± 3.1
$BrNO_2$ + NaI	278	544.2 ± 94.7
	282	335.9 ± 98.9
	285	325.0 ± 92.0
	288	493.8 ± 43.7
	293	349.1 ± 62.2

[a] A typical plot according to eq 20 is shown in Figure 6. The values of $Hk^{1/2}$ are then derived from the corresponding slope. At least four kinetics (i.e., uptake coefficients, see Figure 5) were measured for each $Hk^{1/2}$ value. The given errors are at the 2σ level.

experimental procedures and conditions. Such surface-enhanced reactions were also observed by other groups for Cl_2, Br_2, and $ClONO_2$.[39,40] However, these studies brought stronger evidence of this surface enhancement than our present experiments, since the deviation between our results and eq 13 is weak (the intercept while negative is still close to zero). This gives us little chance to access the potential surface reactivity of $ClNO_2$.

The studies of the uptake rate as a function of temperature showed that the uptake coefficients are temperature independent between 275 and 289 K for all concentrations, whatever the salt.

On NaBr solutions, the main gas-phase product was Br_2 but traces of $BrNO_2$ and BrCl were also observed. It should be noted that the Cl_2, which was always present as a very minor impurity in our nitryl chloride source, also (or mainly since molecular chlorine reacts much faster compared to $ClNO_2$) contributes to the BrCl mass signal. The main product on NaI solutions was I_2, but traces of ICl were also observed. Two mechanisms could explain the observed product. First, $ClNO_2$ may directly react with Br^- or I^- to produce BrCl or ICl, which is then converted into Cl_2 or I_2 according to

$$ClNO_2 + NaX \rightarrow XCl + NaNO_2 \quad (21)$$

$$XCl + NaX \rightarrow X_2 + NaCl \quad (22)$$

Another reaction scheme leading to the same main products would start with an interconversion reaction, i.e.

$$ClNO_2 + NaX \rightarrow XNO_2 + NaCl \quad (23)$$

followed by

$$XNO_2 + NaX \rightarrow X_2 + NaNO_2 \quad (24)$$

With regard to the data obtained, we cannot conclude about the reaction scheme effectively occurring in these aqueous salt solutions. However, to still better understand this chemical system, we further investigated the chemistry of nitryl bromide.

TABLE 4: Uptake Coefficients γ of $BrNO_2$ on Water and Different Salt-Containing Solutions

solution	temp	$(\gamma \pm 2\sigma) \times 10^6$
water	277	2.47 ± 0.20
	281	2.24 ± 0.12
	285	2.37 ± 0.34
	288	2.58 ± 0.41
	293	2.70 ± 0.52
0.5 M NaCl	278	13.25 ± 3.0
	282	9.6 ± 2.3
	285	9.8 ± 2.7
	288	9.7 ± 3.4
	293	14.1 ± 3.0
5×10^{-4} M NaBr	278	8.6 ± 1.3
	282	6.3 ± 1.5
	285	8.2 ± 1.6
	288	11.4 ± 1.9
	293	21.6 ± 10.7
10^{-3} M NaBr	278	24.1 ± 5.8
	282	32.2 ± 11.5
	285	18.0 ± 10.0
	293	26.0 ± 6.7
5×10^{-3} M NaBr	278	56.3 ± 15.3
	282	58.7 ± 17.2
	285	55.3 ± 14.6
	291	65.3 ± 69.3
	293	72.4 ± 38.6
5×10^{-2} M NaBr	278	113.9 ± 26.9
	282	118.3 ± 83.95
	285	160.9 ± 27.5
	293	175.5 ± 26.5
10^{-4} M NaI	278	44.0 ± 2.9
	282	24.2 ± 4.0
	285	44.6 ± 7.1
	288	30.1 ± 2.8
	293	40.1 ± 9.0
2.5×10^{-4} M NaI	278	67.0 ± 9.3
	282	60.1 ± 6.9
	285	57.5 ± 12.5
	288	58.3 ± 10.2
	293	62.0 ± 9.2
5×10^{-4} M NaI	278	169.2 ± 11.5
	282	175.5 ± 8.5
	285	94.1 ± 12.5
	293	129.8 ± 29.8
10^{-3} M NaI	278	203 ± 14
	282	226 ± 12
	285	191 ± 24
	288	198 ± 30
	293	198 ± 53
5×10^{-3} M NaI	278	435 ± 33
	282	301 ± 33
	285	305 ± 31
	288	452 ± 34
	293	370 ± 35

Nitryl Bromide. The uptake of $BrNO_2$ was studied with the wetted-wall technique as a function of temperature (between 276 and 293 K) on different aqueous solutions (i.e., pure water or containing NaCl, NaBr, or NaI). Figure 5 gives a typical first-order plot measured for nitryl bromide on a 10^{-4} M NaI solution. Again, according to eq 19, the slope of the fitted line is a measure of the first-order loss rate k_w from which we determined γ. The complete set of results is listed in Table 4. It should be pointed out that we always observed "pure" first-order losses, which was not the case in the study of Frenzel et al.,[18] where secondary reactions and saturation effects were observed. These effects lead to halogen interconversion reactions that are building back $BrNO_2$ at long interaction times. However, such effects were never observed here, and we always observed, within our experimental errors, pure monoexponential decays. The fact that Frenzel et al. observed secondary reactions and saturation effects, contrarily to our own observations, can

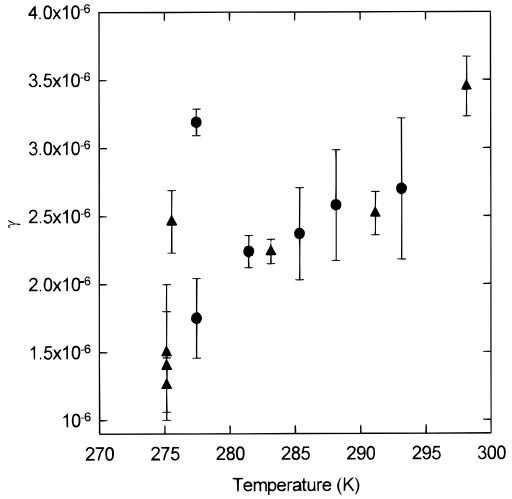

Figure 7. Uptake coefficients for $BrNO_2$ on pure water as a function of temperature. The largest value at 277 K was obtained with higher $BrNO_2$ gas-phase concentration (i.e. about 250 ppm whereas the other experiments were conducted with about 190 ppm). Circles, this work; triangles, Frenzel et al.. (ref 18).

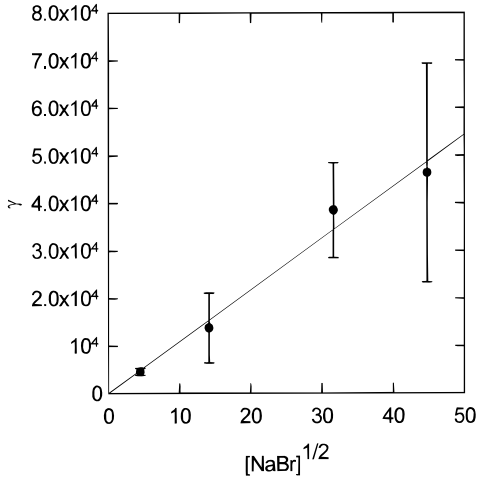

Figure 8. Uptake coefficients for $BrNO_2$ on NaBr solutions according to eq 20 at 293 K.

be related to the time scales of the experiments, i.e., 0.2−5 s for the study performed by Frenzel et al.[18] and 0.05−0.2 s for the present work. Since secondary reactions are only detectable after 0.5−1 s, it is not surprising that our results lead to a simple first-order loss.

The uptake coefficients measured for $BrNO_2$ on pure water were in the range $(1.7-3.2) \times 10^{-6}$ for the temperature varying between 277 and 293 K and exhibit a very small temperature dependence as shown in Figure 7. These values are in excellent agreement with the data reported by Frenzel et al.[18] It should also be noted that these uptake coefficients are about a factor of 2 smaller than those reported for $ClNO_2$;[17] i.e., $BrNO_2$ seems to be less reactive toward water than nitryl chloride. The gas-phase concentration of nitryl bromide also affects its uptake rate by water, and in fact, higher gas-phase concentrations were observed to enhance the uptake rate. This is evidence that the hydrolysis products of $BrNO_2$ will react with this compound and therefore enhance its uptake rate. We identified by ion chromatography that these hydrolysis products are Br^-, NO_2^-, and NO_3^-. Nitrates concentrations were found to be slightly higher than for nitrites but still comparable. The presence of these two species is evidence for two possible $BrNO_2$ hydrolyses

$$BrNO_2 + H_2O \rightarrow HOBr + HONO \quad (25)$$

and

$$BrNO_2 \leftrightarrow NO_2^+ + Br^- \quad (26)$$

$$NO_2^+ + H_2O \rightarrow 2H^+ + NO_3^- \quad (27)$$

or of the reaction with Br^-, i.e.

$$BrNO_2 + Br^- \rightarrow Br_2 + NO_2^- \quad (28)$$

In fact, the presence of bromide or iodide in the solution greatly affected the uptake rate as shown in Figure 8 at 293 K, where the uptake rate increased from 1.7×10^{-6} (on water) to 2.19×10^{-4} on a 5×10^{-2} M NaBr solution. This increase was even larger for iodide owing to its larger reactivity compared to bromide. As already observed for $ClNO_2$, no evident temperature dependence was noticed for these reactive uptake kinetics.

It was found that eq 20 adequately describes the measured uptake coefficients (see Figure 8) enabling us to calculate values for $Hk^{1/2}$ that are listed in Table 3. The uptake coefficients reported for NaBr solutions agree reasonably well with the lower limit reported by Frenzel et al.[18] for the different concentrations.

On pure water and on 0.5 M NaCl solutions, we were not able to identify any gas-phase product, whereas on NaBr and NaI, the main products were Br_2 and I_2, respectively. Traces of IBr were observed, after the interaction of $BrNO_2$ with NaI, but they may have been produced from the reaction of Br_2 (present in our continuous source of nitryl bromide) with NaI.

Discussion and Atmospheric Implications

In Table 5, we summarize literature data in relation to the present work. It can be seen that the agreement between the different studies (when comparable) is relatively favorable. For N_2O_5, the uptake coefficient on "pure" aqueous surfaces is generally reported to be close to $(3^{+3}_{-2}) \times 10^{-2}$, which is in quite good agreement with our average value of 0.018. This latter can also be compared with the recent determination of Hu and Abbatt[41] (and references therein for a more complete description of the uptake of N_2O_5 by sulfuric acid), who measured the uptake coefficient of N_2O_5 on sulfuric aerosols. At high relative humidity (90%), i.e., at low H_2SO_4 content (17 wt %), they measured an average value of 0.023 ± 0.004 and finally only a poor dependence of γ with humidity (i.e., with the H_2SO_4 content). They concluded that water does not play a direct role in the reactive uptake of N_2O_5. They postulated that this compound either surface accommodates or dissociates into NO_2^+ and NO_3^-. The latter possibility corresponds to the chemical scheme generally adopted for concentrated acid solution and recently proposed by Behnke et al.[17] for dilute aqueous solutions for which we found indirect evidence in the present study. When comparing the available data for the uptake on NaX salt and their corresponding solutions, it appears clear that the uptake rate is strongly affected by the amount of water present (as solvent or an adsorbed layer on a solid substrate, i.e., the NaX salt) since the reported uptake coefficients are increasing from about 10^{-4} to 10^{-2} when going from the "dry" solid sample to the dilute aqueous solutions. This may can be taken either as evidence for a rapid reaction between N_2O_5 and water or as proof that some water is needed for its dissociation according to eq 16. With regard to the data obtained in sulfuric acid, other liquid (as H_2SO_4) may induce the ionic dissociation of N_2O_5. Several studies[12,14,15,18,49] also identified the products

TABLE 5: Uptake Coefficients γ of N_2O_5, $ClNO_2$, and $BrNO_2$ on Water and Different Salt-Containing Solutions—A Comparison with Literature Data

	temp (K)	uptake coefficient	ref	notes
N_2O_5 +				
H_2O	271−282	$(6-4) \times 10^{-2}$	30	"pure"
	262−277	$(3-1) \times 10^{-2}$	33	"pure"
	293	$5 \times 10^{-3} < \gamma < 10^{-1}$	31	"pure"
	264−275	1.9×10^{-2}	this work	"pure"
NaCl	300	$>2.5 \times 10^{-3}$	45	dry powders
	223−296	$<10^{-4}$	46	dry powders
	223−296	$(2.4-4.5) \times 10^{-4}$	46	slightly wet powders
	292	3.0×10^{-2}	47	deliquescent aerosol
	263−278	$(3.9-1.4) \times 10^{-2}$	33	1 M solution
	298	$<2.0 \times 10^{-3}$	48	wet salt solutions
		5.0×10^{-4}	49	dry salt
	262−278	1.5×10^{-2}	this work	1 M solution
NaBr (or KBr)		4.0×10^{-3}	49	dry salt
	270−276	1.8×10^{-2}	this work	$(10^{-2}-1)$ M solution
NaI	271−277	$(1.6-2.2) \times 10^{-2}$	this work	(0.1−1) M solution
$ClNO_2$ +				
H_2O	277−291	$(3.4-4.8) \times 10^{-6}$	17	
NaCl	291	$(3.1-0.3) \times 10^{-6}$	17	(0.1−5) M solution
	298	$<10^{-5}$	50	dry substrates
NaBr		1.3×10^{-4}	49	dry substrates
	275−291	$(1.2-4.0) \times 10^{-5}$	18	$(0.5-5) \times 10^{-3}$ M solution
	275	$(1-10) \times 10^{-5}$	37	$(10^{-4}-10^{-2})$ M solution
	275−288	$(7-935) \times 10^{-6}$	this work	$(10^{-4}-1)$ M solution
NaI	268−279	$(1.1-6.6) \times 10^{-3}$	38	$(10^{-3}-10^{-2})$ M solution
	275−288	$(3.1-453) \times 10^{-5}$	this work	$(10^{-4}-10^{-2})$ M solution
$BrNO_2$ +				
H_2O	275−298	$(1.2-3.4) \times 10^{-6}$	17	"pure"
	277−293	$(2.4-2.7) \times 10^{-6}$	this work	"pure"
NaCl	291	$>3.8 \times 10^{-5}$	17	0.5 M solution
	278−293	$(9.6-14.1) \times 10^{-6}$	this work	0.5 M solution
NaBr	291	$>2.2 \times 10^{-5}$	17	$(0.5-1) \times 10^{-2}$ M solution
	278−293	$(6.3-175) \times 10^{-6}$	this work	$(0.5-50) \times 10^{-3}$ M solution
NaI	277−293	$(2.4-45.2) \times 10^{-5}$	this work	$(10^{-4}-(5 \times 10^{-3}))$ M solution

issued from the interactions of N_2O_5 with NaX (wet and dry). The main products are $ClNO_2$, Br_2, and HONO as observed in the present study. Some traces of $BrNO_2$ were observed only over dilute solutions or over solids but at short contact times, which is evidence, as proven here, that $BrNO_2$ is reacting with NaBr. For both nitryl halides, all existing data can be favorably compared as shown in Table 5 and Figure 6. All studies showed that these species react rapidly with NaBr producing Br_2 and HONO as final products through a quite complex chemical scheme.[18]

Frenzel et al.[18] observed, in their study on nitryl bromide, that after long reaction times (i.e., after an important loss of $BrNO_2$) the uptake kinetics were no longer first order. They attributed this observation to the establishment of the following equilibrium:

$$BrNO_2 + Br^- \leftrightarrow Br_2 + NO_2^- \qquad (29)$$

The back-reaction is known to exist since it was used as the source of gaseous $BrNO_2$. However, for our uptake studies the small interaction times used (i.e., smaller than 0.2 s) did not allow a large conversion of $BrNO_2$ to bromine and nitrites. In conjunction with the systematic observation of first-order uptake kinetics with a unique product, we believe that in our study only the forward reaction 28 occurred. We then calculated the corresponding first-order rate constant using our values of the product $Hk^{1/2}$ and Henry's law constant estimated by Frenzel et al.[18] (0.3 M atm^{-1} at 291 K). The values we obtained, at 293 K, are 4.4×10^4 and 1.4×10^6 M^{-1} s^{-1} for the reaction between nitryl bromide and Br^- or I^-, respectively. These reactions may be adequately described as a nucleophilic attack on the slightly positively charged bromine in its nitryl compound. In such a situation, the Swain−Scott equation[42] may be applied, i.e.,

$$\log k_X = sn + \log k_{H_2O} \qquad (30)$$

where k_X is the rate constant for nucleophilic attack of X, k_{H_2O} is the corresponding value for water, n is the nucleophilicity of X, and s is a sensitivity factor. If we calculate the logarithm of the ratio of the two rate constants for Br^- and I^-, we obtain a value of 1.5 that is equal to the difference of the nucleophilicity between bromide and iodide, which are, respectively, 3.5 and 5.0.[42] Therefore eq 30 may be applied with a sensitivity factor of about 1. In Figure 9, we plotted the rate constants according to the Swain−Scott equation and we included the rate constant calculated from the uptake kinetics on water, i.e., 0.33 s^{-1}. All three values seem to be described by eq 30. This would be an indication that the hydrolysis of $BrNO_2$ occurs through a nucleophilic attack of water, i.e., as given in reaction 25. It should be pointed out that the rate constant derived from the small enhancement of the uptake coefficient on a 0.5 M NaCl solution does not fit the description by eq 30. In our study, we were not able to identify any gas-phase product for this reaction (i.e., their concentrations were probably below our sensitivity), but Frenzel et al.[18] showed that the reaction between $BrNO_2$ and Cl^- delivers traces of $ClNO_2$. The existence of this reaction may explain the small increase of the uptake rate we observed.

Concerning nitryl chloride, we observed several products from interactions with bromide-containing solutions. This is an indication that a succession of reactions is occurring. With regard to the data presented here, we cannot definitively conclude about the occurrence or not of one of the two proposed mechanisms (i.e., reactions 21−22 or 23−24). It seems,

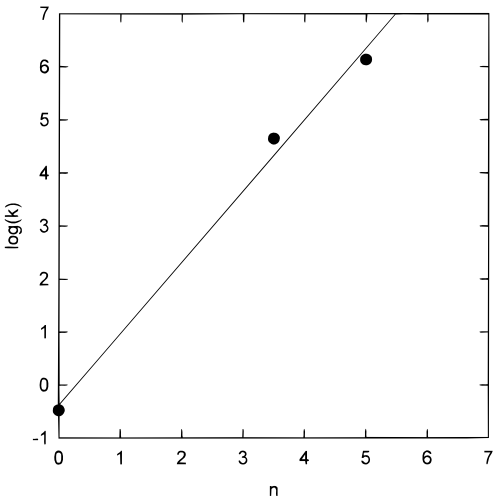

Figure 9. Plot of the logarithm of the rate constant according to the Swain−Scott equation. The nucleophilicity of bromide and iodide are, respectively, 3.5 and 5. [42]

however, that the presence of $BrNO_2$ in the gas phase is an indication that the second reaction scheme is indeed working. Another insight may be gained by considering that the bond between Cl and N in nitryl chloride is nearly purely covalent,[43] i.e., Cl may not be an efficient site for a nucleophilic attack.

Some atmospheric implications of the data presented have been obtained by implementing the box model developed by Sander and Crutzen,[44] describing the heterogeneous chemistry in the marine boundary layer, with the kinetics reported by Behnke et al.,[17] Frenzel et al.,[18] and the present study. If run under polluted conditions (i.e., NO_x concentrations about 10 ppb) with the presence of sea-salt aerosols, the model simulated Cl and Br atom concentrations up to 2×10^4 and 10^5 molecules cm^{-3}. These values are comparable to those actually measured in field campaigns. It should be noted that nitrogen oxide chemistry is not the unique pathway for converting stable ions (Cl^- and Br^-). Other reactions as, for example, with Caro's acid may be a source of halogenated radicals. Nevertheless, halogen radical activation through the reactions of N_2O_5 and subsequently of the nitryl compounds is by far the most rapid way for producing Cl and Br atoms, but it requires high NO_x concentrations, which can only be encountered in polluted coastal regions.

Conclusion

We studied the uptake kinetics of N_2O_5, $ClNO_2$, and $BrNO_2$ with either the droplet train or wetted-wall flow tube techniques. The uptake of N_2O_5 was found to be independent of the composition of the aqueous phase which was taken as evidence for a unimolecular dissociation of hydrated N_2O_5. When reacting with chloride or bromide several photoactive products were observed, i.e., $ClNO_2$, $BrNO_2$, and Br_2. The uptake kinetics of the nitryl compounds were shown to be highly dependent on the composition of the aqueous phase. Nitryl chloride was shown to produce $BrNO_2$ and Br_2 when reacting with Br^-, whereas nitryl bromide was converted into Br_2. The kinetics and products were in good agreement with existent data.

Acknowledgment. We are grateful to V. Scheer and A. Frenzel for helpful discussion concerning the synthesis of nitryl bromide. We also thank A. Geyer and B. Schaffner, the glassblowers of the chemistry department, for their help in handling and producing our glass setup. Support of this study by the EU (Project SALT, Grant ENV4-CT95-0037) and by the CNRS (Programme National de Chimie Atmosphérique, PNCA) is gratefully acknowledged.

References and Notes

(1) Finlayson-Pitts, B. J.; Pitts, J. N., Jr. *Atmospheric Chemistry: Fundamentals and Experimental Techniques*; John Wiley & Sons: New York, 1986.

(2) Martens, C. S.; Wesolowski, J. J.; Harriss, R. C.; Kaifer, R. *J. Geophys. Res.* **1973**, *78*, 8778.

(3) Hitchcock, D. R.; Spiller, L. L.; Wilson, W. E. *Atmos. Environ.* **1980**, *14*, 165.

(4) Keene, W. C.; Pszenny, A. A. P.; Jacob, D. J.; Duce, R. A.; Galloway, J. N.; Schultz-Tokos, J. J.; Sievering , H.; Boatman J. F. *Global Biogeochem. Cycles* **1990**, *4*, 407.

(5) Pszenny, A. A. P.; Keene, W. C.; Jacob, D. J.; Fan, S.; Maben, J. R.; Zetwo, M. P.; Springer-Young, M.; Galloway J. N. *Geophys. Res. Lett.* **1993**, *20*, 699.

(6) Wingetener, O. W.; Kubo, M. K.; Blake, N. J.; Smith Jr., T. W.; Blake, D. R.; Rowland, F. S. *J. Geophys. Res.* **101**, 1996, 4331.

(7) Fan, S.-M.; Jacob, D. J. *Nature* **1992**, *359*, 522.

(8) Mozurkewich, M. *J. Geophys. Res.* **1995**, *100*, 14199.

(9) Finlayson-Pitts, B. J.; Ezell, M. J.; Grant, C. E. *J. Phys. Chem.* **1986**, *90*, 17.

(10) Ganske, J. A.; Ezell M. J.; Berko, H. N.; Finlayson-Pitts B. J. *Chem. Phys. Lett*. **1991**, *179*, 204.

(11) Zetzsch C.; Behnke W. *Ber. Bunsen-Ges. Phys. Chem*. **1992**, *96*, 488.

(12) Finlayson-Pitts, B.; Johnson, S. *Atmos. Environ.* **1988**, *22*, 1107.

(13) Junkermann, W.; Ibusuki, T *Atmos. Environ.* **1992**, 26, 3099.

(14) Fenter, F. F.; Caloz, F.; Rossi, M. J. *J. Phys. Chem.* **1994**, *98*, 9801.

(15) Laux, J. M.; Hemminger, J. C.; Finlayson-Pitts, B. J. *J. Geophys. Res. Lett.* **1994**, *21*, 1623.

(16) Vogt, R.; Finlayson-Pitts, B. J. *Geophys. Res. Lett.* **1994**, *21*, 2291.

(17) Behnke, W.; George, C.; Scheer, V.; Zetzsch, C. *J. Geophys. Res.* **1997**, *102*, 3795.

(18) Frenzel, A.; Scheer, V.; Sikorski, R.; George, Ch.; Behnke, W.; Zetzsch, C. *J. Phys. Chem. A* **1997**, *102*, 1329.

(19) Magi, L.; Schweitzer, F.; Pallares, C.; Cherif, S.; Mirabel, Ph.; George, Ch. *J. Phys. Chem.* **1997**, *101*, 4943.

(20) Worsnop. D. R.; Zahniser, M. S.; Kolb, C. E.; Gardner, J. A.; Watson, L. R.; Van Doren, J. M.; Jayne, J. T.; Davidovits, P. *J. Phys. Chem.* **1989**, *93*, 1159−1172.

(21) Danckwerts, P. *Gas−Liquid Reactions*; Chemical Engineering Series; McGraw Hill: New York, 1970.

(22) Cooney, D. O.; Kim, S.; Davis, E. J. *J. Chem. Eng. Sci.* **1974**, *29*, 1731.

(23) Murphy, D. M.; Fahey D. W. *Anal. Chem.* **1987**, *59*, 2753.

(24) Brown, R. L. *J. Res. Nat. Bur. Stand. (U.S.)* **1978**, 83, 1.

(25) Colburn, C. B. *Developments in Inorganic Nitrogen Chemistry*; Elsevier: Amsterdam, 1973; Vol. 2.

(26) Scheffler, D.; Grothe, H.; Willner, H.; Frenzel, A.; Zetzsch, C. *Inorg. Chem.* **1997**, *36*, 335.

(27) Tevault, D. E. *J. Phys. Chem.* **1979**, *83*, 2217.

(28) Feuerhahn, M.; Minkwitz, R.; Engelhardt, U. *J. Mol. Spectrosc.* **1979**, *77*, 429.

(29) Reid, R. C.; Prausnitz, J. M.; Poling, B. E. *The Properties of Gases and Liquids*, 4th ed.; McGraw-Hill: New York, 1987.

(30) VanDoren, J. M.; Watson, L. R.; Davidovits, P.; Worsnop, D. R.; Zahniser, M. S.; Kolb, C. E. *J. Phys. Chem.* **1990**, *94*, 3265.

(31) Kirchner, W.; Welter, F.; Bongartz, A.; Kames, J.; Schweighoefer, S.; Schurath, U. *J. Atmos. Chem.*, **1990**, *10*, 427.

(32) Behnke, W.; Krüger, H.-U.; Scheer, V.; Zetzsch, C. *J. Aerosol Sci*. **1992**, *S23*, 933.

(33) George, Ch.; Ponche, J. L.; Mirabel, Ph.; Behnke, W.; Scheer, V.; Zetzsch, C. *J. Phys. Chem.* **1994**, *98*, 8780.

(34) Kolb, C. E.; Worsnop, D. R.; Zahniser M. S.; Davidovits, P.; Hanson, D. R.; Ravishankara A. R.; Keyser, L. F.; Leu, M. T.; Williams, L. R.; Molina, M. J.; Tolbert, M. A. *Laboratory Studies of Atmospheric Heterogeneous Chemistry*; Current Problems in Atmospheric Chemistry; Barker, J. R., Ed.; Advances in Physical Chemistry Series; World Scientific: Singapore, 1994; Vol. 3, pp 771−875.

(35) Mozurkewich, M.; Calvert, J. G. *J. Geophys. Res.*, **1988**, *93*, 889.

(36) Fried, A.; Henry, B. E.; Calvert, J. G.; Mozurkewich, M. *J. Geophys. Res.* **1994**, *99*, 351.

(37) Crowley, J.; Fickert, S. Personal communication.

(38) George, Ch.; Behnke, W.; Scheer, V.; Zetzsch, C.; Magi, L.; Ponche, J. L.; Mirabel, Ph. *Geophys. Res Lett.* **1995**, *22*, 1505.

(39) Hu, J. H.; Shi, Q.; Davidovits, P.; Worsnop, D. R.; Zahniser, M. S.; Kolb, *C. E. J. Phys. Chem.* **1995**, 99, 8768.

(40) Hanson, D. R.; Ravishankara, A. R. *J. Phys. Chem.* **1994**, *98*, 8. 5728.

(41) Hu, J. H.; Abbatt, J. P. D. *J. Phys. Chem. A* **1997**, *101*, 871.

(42) Swain, C. G.; Scott, C. B. *J. Am. Chem. Soc*. **1953**, *75*, 141. See also: March, J. *Advanced Organic Chemistry*, 4th ed.; John Wiley & Sons Inc.: New York, 1992.

(43) Obermeyer, A.; Borrmann, H.; Simon, A. *J. Am. Chem. Soc.* **1995**, *117*, 7887.

(44) Sander, R.; Crutzen, P. J. *J. Geophys. Res.* **1996**, *101*, 9121.

(45) Livingstone, F. E.; Finlayson-Pitts, B. J. *Geophys. Res. Lett.* **1991**, *18*, 17.

(46) Leu, M. T.; Timonen, R. S.; Keyser, L. F.; Yung, Y. L. *J. Phys. Chem.* **1995**, *99*, 13203.

(47) Zetzsch, C.; Behnke, W. *Ber. Bunsen-Ges. Phys. Chem.* **1992**, *96*, 488.

(48) Msibi, I. M.; Li, Y.; Shi, J. P.; Harrison, R. M. *J. Atmos. Chem.* **1994**, *18*, 291.

(49) Caloz, F. Laboratory Kinetic Studies of Heterogeneous Processes Relevant to the Marine Troposhere. Ph.D. Thesis, Ecole Polytechnique de Lausanne, Switzerland, 1997.

(50) Beichert P.; Finlayson-Pitts, B. J. *J. Phys. Chem*. **1996**, *100*, 15218.